The acyclotide ribe 31 from *Rinorea bengalensis* has selective cytotoxicity and potent insecticidal properties in *Drosophila*

Received for publication, February 21, 2022, and in revised form, August 16, 2022 Published, Papers in Press, August 22, 2022,
https://doi.org/10.1016/j.jbc.2022.102413

Tien T. Dang[1], Yen-Hua Huang[1], Stanislav Ott[2], Peta J. Harvey[1], Edward K. Gilding[1], Benjamin J. Tombling[1], Lai Y. Chan[1], Quentin Kaas[1], Adam Claridge-Chang[2,3,4], and David J. Craik[1,*]

*From the [1]Institute for Molecular Bioscience, Australian Research Council Centre of Excellence for Innovations in Peptide and Protein Science, The University of Queensland, Brisbane, Queensland, Australia; [2]Program in Neuroscience and Behavioral Disorders, Duke-NUS Medical School, Singapore, Singapore; [3]Institute for Molecular and Cell Biology, A*STAR, Singapore; [4]Department of Physiology, National University of Singapore, Singapore, Singapore*

Edited by Wolfgang Peti

Cyclotides and acyclic versions of cyclotides (acyclotides) are peptides involved in plant defense. These peptides contain a cystine knot motif formed by three interlocked disulfide bonds, with the main difference between the two classes being the presence or absence of a cyclic backbone, respectively. The insecticidal activity of cyclotides is well documented, but no study to date explores the insecticidal activity of acyclotides. Here, we present the first *in vivo* evaluation of the insecticidal activity of acyclotides from *Rinorea bengalensis* on the vinegar fly *Drosophila melanogaster*. Of a group of structurally comparable acyclotides, ribe 31 showed the most potent toxicity when fed to *D. melanogaster*. We screened a range of acyclotides and cyclotides and found their toxicity toward human red blood cells was substantially lower than toward insect cells, highlighting their selectivity and potential for use as bioinsecticides. Our confocal microscopy experiments indicated their cytotoxicity is likely mediated *via* membrane disruption. Furthermore, our surface plasmon resonance studies suggested ribe 31 preferentially binds to membranes containing phospholipids with phosphatidyl-ethanolamine headgroups. Despite having an acyclic backbone, we determined the three-dimensional NMR solution structure of ribe 31 is similar to that of cyclotides. In summary, our results suggest that, with further optimization, ribe 31 could have applications as an insecticide due to its potent *in vivo* activity against *D. melanogaster*. More broadly, this work advances the field by demonstrating that acyclotides are more common than previously thought, have potent insecticidal activity, and have the advantage of potentially being more easily manufactured than cyclotides.

Cyclotides have attracted interest as next-generation therapeutics and agricultural agents due to their unique topology and diverse biological activities (1–3). These plant-derived peptides comprise a head-to-tail cyclic backbone of 28 to 37 amino acids and three intramolecular disulfide bonds. Together with the cyclic backbone, the three disulfide bonds form a structure known as the cyclic cystine knot (CCK) motif, which bestows cyclotides with exceptional resistance to proteolytic, thermal, or chemical degradation (1, 4).

Cyclotides are divided into three main subfamilies: Möbius, bracelet, and trypsin inhibitor. The Möbius and bracelet subfamilies are distinguished by the presence or absence of a *cis* Xaa-Pro bond in loop 5, respectively (1). Cyclotides from the trypsin inhibitor family retain the CCK motif but have low sequence similarity and different biological activities to either Möbius or bracelet cyclotides (5).

Host defense has been widely considered as the main function of cyclotides in plants (6, 7). This function has stimulated interest in the use of cyclotides for agricultural applications, which is supported by their wide range of biological activities, including antimicrobial (8–10), antifouling (11), cytotoxic (12), insecticidal (13), and molluscicidal activities (14). For example, the prototypic Möbius cyclotide kalata B1, discovered from *Oldenlandia affinis*, causes significantly reduced growth of *Helicoverpa punctigera*—a major pest of corn and cotton (Fig. 1*A*) (15). Similarly, a recent study showcased the activity of the prototypic bracelet cyclotide cycloviolacin O2 (cyO2) against *Myzus persicae* probing and feeding behavior (16). The bioinsecticide Sero-X (https://innovate-ag.com.au/sero-x/) is produced from an extract of the cyclotide-bearing plant *Clitoria ternatea* (Fabaceae) and was recently approved for agricultural use against various insect pests including *Helicoverpa* species, green mirids, green vegetable bugs, and whiteflies. The cyclotide Cter M, isolated from *C. ternatea* (Fig. 1*B*) (17), displays insecticidal activity against the cotton bollworm *Helicoverpa armigera*, suggesting it may be responsible for the activity of Sero-X. Peptide-based bioinsecticides offer potential advantages over traditional pesticides of lower off-target toxicity, reduced environmental impacts, and more sustainable manufacture.

Recently, noncyclic analogs of cyclotides, called acyclotides, have attracted increasing attention (18, 19). Acyclotides have a similar sequence to cyclotides and also contain a cystine knot but lack a head-to-tail cyclic backbone. The backbone cyclization is absent due to a stop codon occupying the position that would encode an Asx (Asn or Asp) residue in a typical

* For correspondence: David J. Craik, d.craik@imb.uq.edu.au.

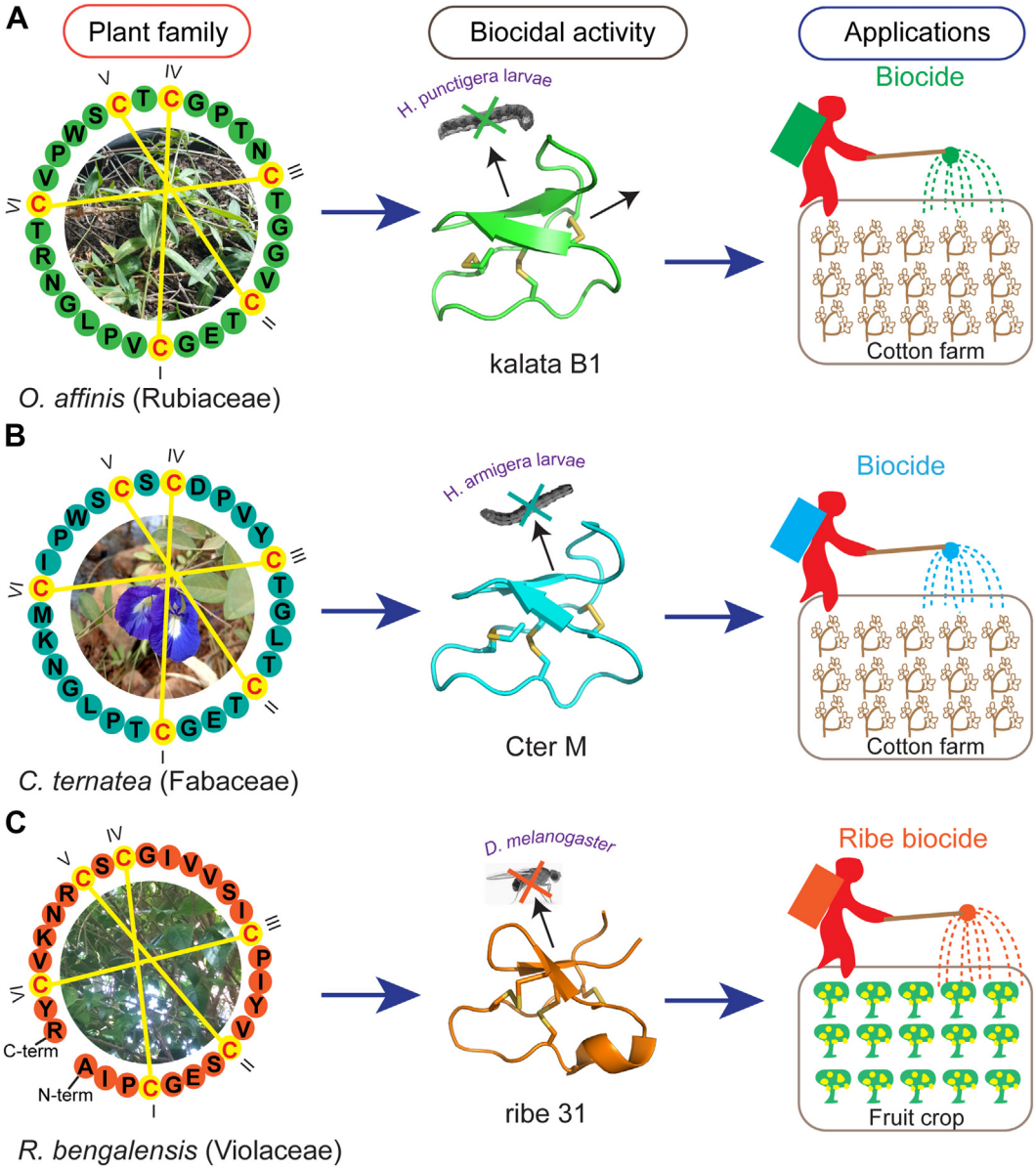

Figure 1. Insecticidal activity of kalata B1, Cter M, and ribe 31 against different insects. *A*, sequence and insecticidal activity of kalata B1 against *Helicoverpa punctigera*, major pests of corn and cotton. *B*, sequence and insecticidal activity of Cter M against *Helicoverpa armigera* larvae (*H. armigera*), a cotton pest. *C*, sequence and insecticidal activity of ribe 31 against *Drosophila melanogaster* (*D. melanogaster*). Cysteine residues are marked *red* in *yellow* circles. *Yellow* lines connecting two cysteine residues represent disulfide bonds.

cyclotide precursor (20). This key Asx residue and an adjacent C-terminal tail peptide in the precursor facilitate cyclization in cyclotides by asparaginyl endopeptidase enzymes in plants (19, 21). Despite their acyclic backbone, acyclotides have comparable stability and structures to cyclotides, primarily due to the stabilizing effect of the cystine knot motif (20, 22). Apart from local changes at the terminal residues, the NMR structures of two acyclotides, violacin A, and MCoTI-V have shown that linearization has negligible effects upon the structure of the cystine knot core (22, 23). Examination of species from the five dicot families known to produce cyclotides (namely the Violaceae, Rubiaceae, Solanaceae, Cucurbitaceae, and Fabaceae) suggests that fewer acyclotides than cyclotides are produced by these plants (24, 25). Some monocots from the Poaceae family express acyclotides but no cyclotide has so far been discovered in this plant family (19), despite these plants containing asparaginyl endopeptidase enzymes. Although acyclotides host features common to the bracelet or Möbius cyclotide subfamilies, they are topologically linear. Examples include violacin A (Möbius subfamily) (22), kalata B9 (bracelet subfamily) (26), and modi 6 (trypsin inhibitor subfamily) (27). Overall, there are currently around 105 acyclotides reported with about 85% of them being homologous to bracelet subfamily cyclotides. Due to their apparent scarcity in nature compared to cyclotides, the biological activities of acyclotides have been less extensively studied. Specifically, there have been no reported studies assessing the insecticidal activities of acyclotides, highlighting this as an unexplored research field.

Pesticides are a keystone in the agricultural sector, and the need for developing alternative insecticidal compounds is becoming increasingly apparent due to the negative environmental impacts of many existing pesticides (28). Some widely used conventional insecticides are composed of chemicals that cause environmental damage to surroundings and can pose health risks to the wider population (29). For instance, there have been reports of residual insecticides leading to increased cancer risk (30) and poisoning (31). Thus, environmentally friendly insecticides, such as Sero-X, are attractive alternatives to harsh chemicals, potentially helping to reduce contamination and damage to ecosystems.

Drosophila suzukii is a major fruit pest in the North America and Asia (32) and is closely related to the vinegar fly *Drosophila melanogaster*, which is widely used in the laboratory as a model organism for biological studies, that is, toxicity, persistent behavior, aging, cellular morphogenesis, and human disease modeling (33, 34), as well as for testing behavior and phenotype effects of insecticides (35–38). *D. melanogaster* has also been used to study insecticide resistance (39, 40).

In the current study, a family of acyclotides previously discovered from the stem and leaf of *Rinorea bengalensis*, named ribe peptides (20), were isolated and evaluated for their potential insecticidal activity. The toxicity of these peptides was examined against two insect cell lines *in vitro* and tested for *in vivo* insecticidal activity against *D. melanogaster* (Fig. 1*C*). Ribe 31 was found to be more toxic than the well-characterized insecticidal cyclotide kalata B1. Structural analysis revealed that all ribe peptides display a similar cystine knot motif and tertiary structure to cyclotides. Ribe 31 was shown to bind preferentially to a model membrane containing phospholipids with phosphatidyl-ethanolamine (PE) headgroups, suggesting that its ability to disrupt membrane is related to its insecticidal activity. Our results suggest that ribe 31 is a useful lead for the development of ecofriendly biocides for crop protection.

Results

Isolation of cystine knot peptides from R. bengalensis

Ribe peptides isolated from stem and leaf tissue extracts of *R. bengalensis* were purified and separated based on their hydrophobicity as evaluated by their elution times in reverse-phase HPLC (RP-HPLC) (Fig. 2*A*). Generally, peaks with a later elution time are more hydrophobic. From early to late elution, the order of hydrophobicity was acyclotides ribe 10, 20, 24, and 31, and cyclotide ribe 33. Amino acid sequences of the isolated peptides are shown in Fig. 2*B*.

In vivo *toxicity of ribe peptides to* D. melanogaster *after oral feeding*

In vitro assays indicated that several purified peptides (ribe 10, 20, 24, 31, 33) and the stem extract from *R. bengalensis* had cytotoxic activity against insect cells (Table 1). The *in vivo* insecticidal activity of these peptides for *D. melanogaster* were

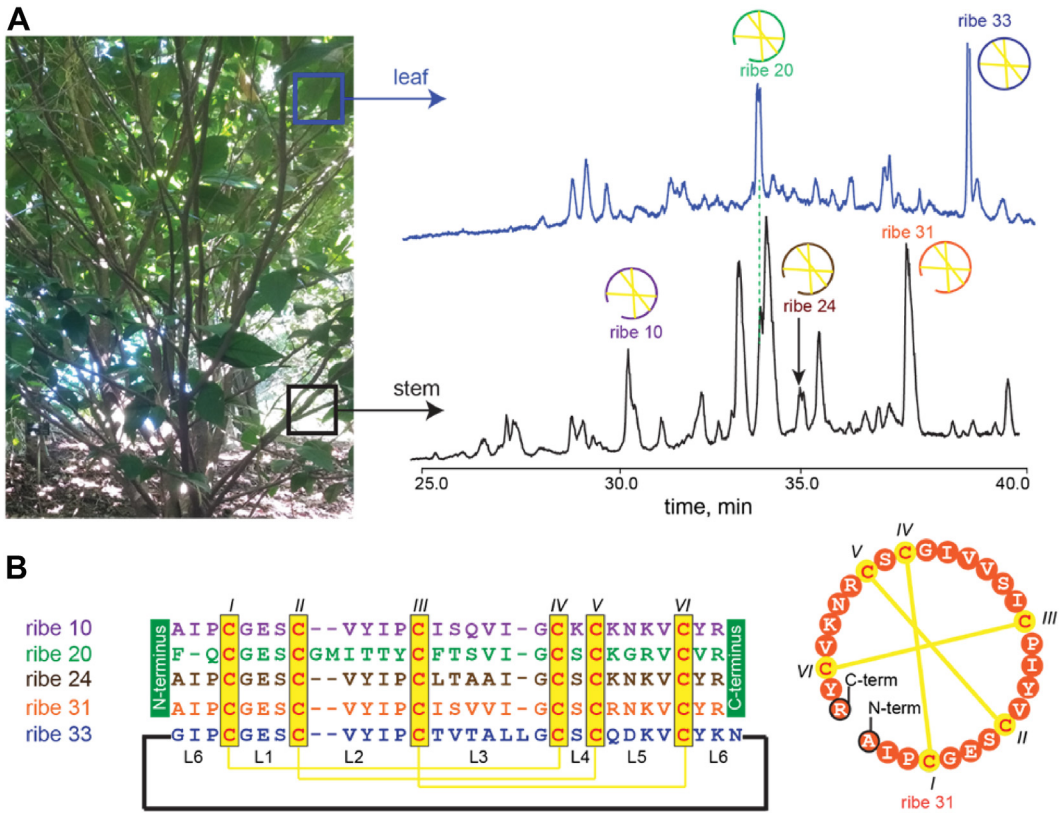

Figure 2. Cystine knot peptides derived from *R. bengalensis*. *A*, HPLC traces of stem and leaf extracts of *R. bengalensis* and the relative elution time of cystine knot peptides discovered from it are shown in top panel. *B*, the amino acid sequences of acyclotides ribe 10, 20, 24, and 31 and cyclotide ribe 33 are listed in the bottom panel. *Yellow* lines connecting two cysteine residues represent disulfide bonds.

Table 1
Cytotoxicity and hemolytic activity of isolated peptides against insect cell lines (Sf9 and High Five) and red blood cells

Peptide	CC_{50} (μM) ± SEM[a]		
	Sf9[b]	High five[c]	RBC[d]
ribe 10	0.8 ± 0.0	1.3 ± 0.1	14.0 ± 0.2
ribe 20	3.5 ± 0.1	8.3 ± 0.1	>25
ribe 24	0.3 ± 0.0	0.9 ± 0.1	11.3 ± 0.1
ribe 31	0.7 ± 0.0	2.6 ± 0.1	21.4 ± 0.2
ribe 33	1.6 ± 0.1	3.2 ± 0.1	21.9 ± 0.2
stem extract	0.3 ± 0.0	0.7 ± 0.1	N.D.
kalata B1	3.2 ± 0.1	N.D.	8.4 ± 0.1
cyO2	0.2 ± 0.0	1.0 ± 0.0	22.0 ± 0.2

[a] Cytotoxic concentration required to kill 50% of the cells (CC_{50}) with data representing the SEM from triplicates.
[b] Sf9: a clonal isolate derived from *Spodoptera frugiperda* Sf21 cells.
[c] High Five: an insect cell line originating from the ovarian cells of the cabbage looper, *Trichoplusia ni*.
[d] N.D.: not determined due to insufficient samples.

evaluated and compared to known insecticidal cyclotides cyO2 and kalata B1. Initial screening involved feeding flies with stem extracts (50 μg), ribe peptides (16 μM), or 10% sucrose (vehicle control) using the capillary feeder (CAFE) assay (Fig. S1, Supporting Information). In this screen, only ribe 31 caused a reduction in lifespan.

Subsequently, multiple concentrations of ribe 31 were tested to determine a dose–response relationship. As shown in Fig. 3*A*, the lifespan of the flies was shorter with increasing peptide concentrations. When ribe 31 was administered at 1.6, 16, and 160 μM, the average fly survival decreased by −200, −252, and −352 h, respectively. This average survival rate was drastically lower than that for control flies (average survival of 458 h). Thus, these results confirm that the administration of ribe 31 shortened the lifespan of *D. melanogaster* in a dose–response manner, with concentrations as low as 1.6 μM, provoking substantial toxicity. Cyclotides cyO2 and kalata B1 have previously been shown to be effective on *M. persicae* (16) and to impair the growth and development of *H. punctigera*, respectively (15). To extend our understanding of toxicity to the Diptera order of insects, cyO2 and kalata B1 were tested on vinegar flies here, and it was found that lifespan declined with increasing concentrations of cyO2 and kalata B1. However, the toxic effect of cyO2 was not as strong as that of ribe 31, as cyO2 administered at 1.6, 16, and 160 μM reduced average survival by −137, −174 and −310 h, respectively (Fig. 3*B*). In addition, the effect of kalata B1 on survival was weaker; the average survival reduction was −39, −99, and −140 h when administered at 1.7, 17, and 170 μM, respectively (Fig. 3*C*). More details on the side-by-side comparison of ribe 31 *versus* cyO2 or kalata B1 on fly survival are shown in Fig. 2.

Structural analysis of ribe 10, 20, 24, and 31

The secondary structure elements of the ribe peptides were evaluated by measuring their secondary Hα NMR chemical shifts (*i.e.*, the difference of measured shifts from random coil values). These shifts were compared to those of cyO2, which also belongs to the bracelet cyclotide subfamily (Fig. 4*A*) (41). Overall, the ribe peptides showed similar secondary shifts to cyO2, indicating that all the peptides have similar secondary structure elements. Slight differences were observed between the ribe peptides in the loops that showed sequence variability. In particular, the different loop lengths and sequences of ribe 20 result in chemical shift differences compared to the other ribe acyclotides, in loops 3, 5, and 6 (Fig. S3, Supporting Information). The amino acid sequence of loop 3 was variable among the studied peptides, and the corresponding Hα shifts were also different, suggesting different conformations.

To determine the effect of an acyclic backbone on structure, the three-dimensional structure of ribe 31 was determined based on NMR spectroscopy measurements. A total of 326 distance restraints and 32 dihedral angle restraints was used to calculate preliminary structures with the following imposed disulfide connectivities: Cys4-Cys20, Cys8-Cys22, and Cys13-Cys27. Both proline residues in loops 2 and 6 were determined to adopt a *trans* conformation based on strong Hδ(*i*) Pro-Hα(*i*-1) NOEs. Amide temperature coefficients identified six residue pairs involved in hydrogen bond interactions (Cys4 HN–Cys27 O, Ser21 HN–Tyr28 O, Arg23 HN–Val 26 O, Cys27 HN–Glu6 O, Tyr28 HN–Ser21 O, and Arg29 HN–Ile2 O). The final ensemble of structures (Fig. 4*B*) is well defined with an average pairwise RMSD across backbone atoms of 0.71 Å. The models were of very good quality as evidenced by an average MolProbity score of 1.8 (Table S2). Despite the linear nature of ribe 31, its backbone structure overlays well with that of cyO2 (RMSD 0.90 Å) with conservation of the three stranded antiparallel β-sheet, hydrogen bonding network across the core, and a short α-helix in loop 3 (Fig. 4*C*).

Homology modeling of ribe peptides

Homology models of all tested peptides are illustrated in Fig. 5*A* as ribbon (left) and surface (right) representations. Analyzing the surface properties of the ribe peptides from the models visualizes the distribution of the hydrophobic patches that derive from residues in loops 2 and 3. Compared to ribe 10 and 20, ribe 24, 31, and 33 have an additional hydrophobic residue in their loop 3. The models suggest that loop 3 drives the difference in hydrophobicity between the peptides. Ribe 24, 31, and 33 indeed have longer HPLC retention times than the other two ribe peptides (10 and 20, see Fig. 2*A*). The more hydrophobic ribe peptides 24, 31, and 33 were expected to bind with higher affinity to lipid membranes than ribe 10 and ribe 20, as later tested using surface plasmon resonance (SPR).

Cytotoxicity of ribe peptides against insect cells

To assess the potency of the ribe peptides as insecticidal agents, their activity against two pest insect cell lines was tested using the 3-(4,5-dimethylthiazol-2-yl)-2,5-diphenyltetrazolium bromide (MTT) assay. In experiments comparing selected peptides to an extract, the stem extract from *R. bengalensis* (5 mg/ml) containing a plethora of acyclotides was shown to be toxic to both insect cell lines (Table 1), suggesting that the plant-expressed peptides are potentially cytotoxic. Isolated ribe peptides had different levels of cytotoxicity toward the two insect cell lines, as shown in Table 1. Ribe 10, ribe 24, and ribe 31 had higher toxicity against Sf9

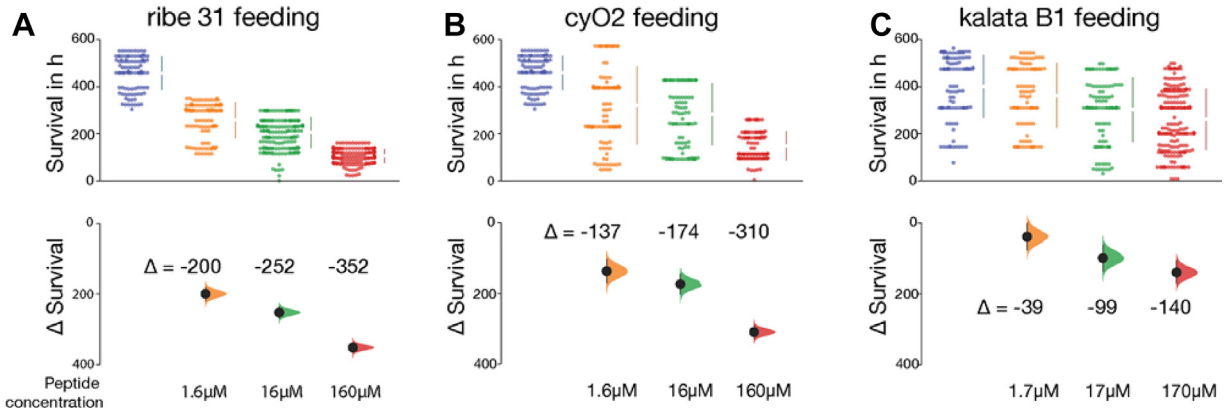

Figure 3. The results of a CAFE assay of ribe 31 (*A*), cyO2 (*B*), and kalata B1 (*C*) on *D. melanogaster* at a range of concentrations (μM). The lifespan of flies fed a sucrose diet (20% sucrose) or a sucrose plus ribe 31 diet at varying concentrations is shown at the top. Differences in average lifespan of each experimental group compared to the sucrose-only control group ('sucrose') are shown at the bottom. Each dot in the scatter plot represents the survival of one fly. Error bars show the 95% CI. *A*, effect size statistics: ribe 31, 1.6 μM (n = 98) *versus* sucrose (n = 104) = −200 [95% CI −220, −180] $p < 1*10$ to 4; ribe 31, 16 μM (n = 207) *versus* sucrose (n = 104) = −252 [95% CI −269, −236] $p < 1*10$ to 4; ribe 31, 160 μM (n = 209) *versus* sucrose (n = 104) = −352 [95% CI −365, −337] $p < 1*10$ to 4. *B*, effect size statistics: cyO2, 1.6 μM (n = 105) *versus* sucrose (n = 104) = −137 [95% CI −171, −103] $p < 1*10$ to 4; cyO2, 16 μM (n = 105) *versus* sucrose (n = 104) = −174 [95% CI −202, −146] $p < 1*10$ to 4; cyO2, 160 μM (n = 105) *versus* sucrose (n = 104) = −310 [95% CI −327, −291] $p < 1*10$ to 4. *C*, effect size statistics: kalata B1, 1.7 μM (n = 99) *versus* sucrose (n = 102) = −39 [95% CI −76, 0] $p = 0.0327$; kalata B1, 17 μM (n = 105) *versus* sucrose (n = 102) = −99 [95% CI −136, −62] $p < 1*10$ to 4; kalata B1: 170 μM (n = 207) *versus* sucrose (n = 102) = −140 [95% CI −170, −106] $p < 1*10$ to 4. CI, confidence interval.

cells, whereas ribe 20 was the least toxic to both insect cell lines. The grand average of hydropathy (42) score, which is the average Kyte–Doolittle hydropathy score for each residue of an amino acid sequence, was computed for each peptide. According to this score, the two most cytotoxic acyclotides, ribe 31 and 24, are also the most hydrophobic (Table S1, Supporting Information). In general, all the ribe peptides showed greater toxicity to High Five cells than to Sf9 cells. The

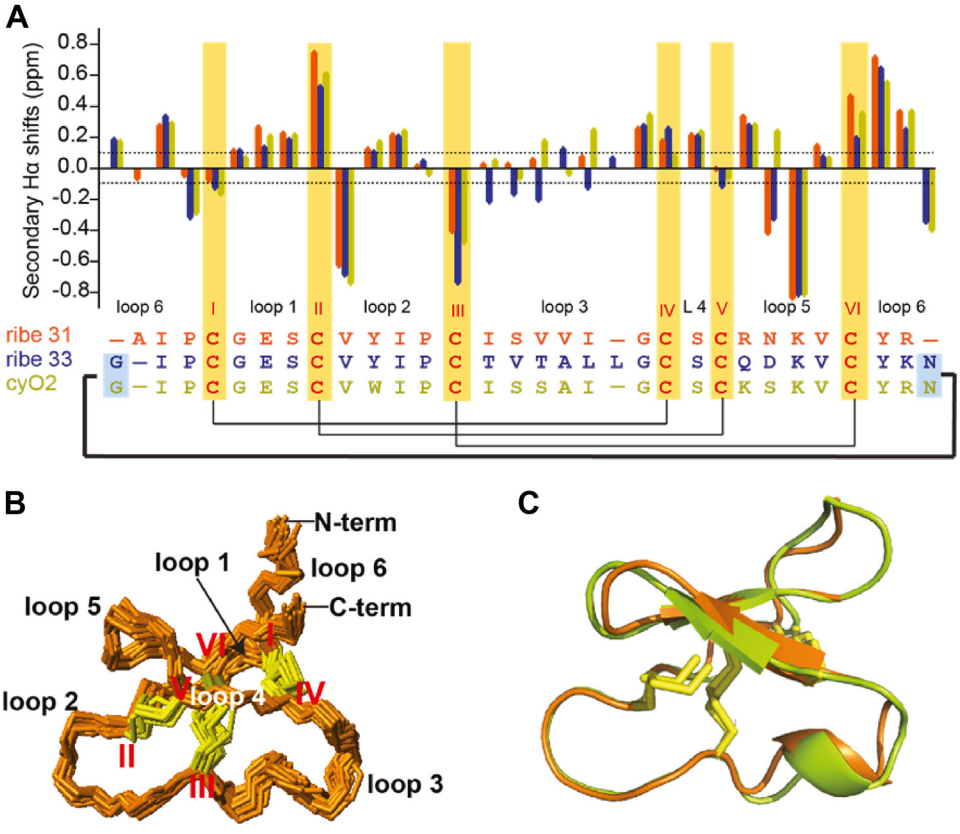

Figure 4. Secondary Hα chemical shift comparison between cyO2 and ribe 31 and 33 and the three-dimensional NMR structure of ribe 31. *A*, the comparison of secondary Hα chemical shifts of ribe 31 (*orange*), ribe 33 (*blue*) and cyO2 (*lime green*). The chemical shifts of cyO2 were obtained from the Biological Magnetic Resonance Data Bank (BMRB, ID: 16073 (62)). All cysteines are highlighted in *red* text with *yellow* boxes. The cyclic backbones of ribe 33 and cyO2 are indicated with a thick *black* line, and disulfide bond connectivities ($Cys^{I\text{-}IV}$, $Cys^{II\text{-}V}$ and $Cys^{III\text{-}VI}$) are shown as thin *black* lines. *B*, superposition of 20 conformers representing the 3D NMR structure of acyclotide ribe 31. *C*, the superimposition of 3D NMR structure of cyclotide cyO2 (*lime green*) and acyclotide ribe 31 (*orange*).

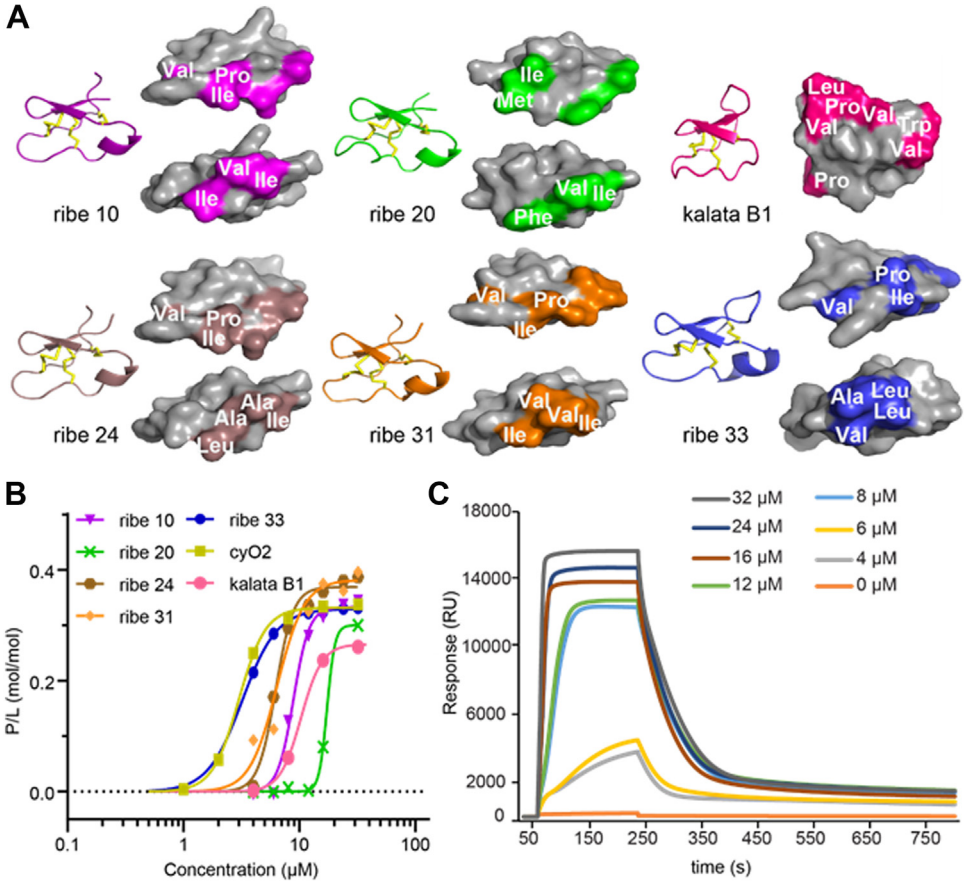

Figure 5. Homology model and binding affinity of ribe peptides toward the model membrane. *A*, homology models of kalata B1 (*pink*), ribe 10 (*purple*), ribe 20 (*green*), ribe 24 (*brown*), ribe 31 (*orange*), and ribe 33 (*blue*) generated using the SWISS-MODEL web server (https://swissmodel.expasy.org) using the structure of cyO2 (PDB ID: 2KCG) as a template. All structures are represented in surface diagrams using PyMol, with the hydrophobic residues highlighted in corresponding colors. *B*, binding affinity of ribe peptides toward the model membrane composed of POPC/POPE (80:20) evaluated using surface plasmon resonance. *C*, sensorgrams of ribe 31 binding to the model membrane at a range of concentrations from 4 μM to 32 μM. PDB, Protein Data Bank; POPC, 1-palmitoyl-2-oleoyl-glycero-3-phosphocholine; POPE, 1-palmitoyl-2-oleoyl-sn-glycero-3-phosphoethanolamine.

toxicity of the ribe peptides is similar to that of insecticidal cyclotides cyO2 and kalata B1 (43, 44). To determine whether the peptides demonstrated toxicity against red blood cells (RBCs), the hemolytic activities of the five ribe peptides were tested (Table 1). The isolated peptides showed 3 to 12-fold lower toxicity toward human RBCs compared to insect cells.

Confocal analysis

Sf9 insect cells were treated with ribe 31 (1 μM), and cell death was monitored with time-lapse microscopy in the presence of SYTOX Green over a 4 h period. SYTOX Green is a fluorescent nucleic acid stain that is impermeable to live cells but penetrates cells with compromised plasma membranes. From the time-lapse movie, Sf9 cells treated with ribe 31 became fluorescent over the course of the experiment, indicating that cell death is associated with membrane disintegration. The observed toxicity of ribe 31 agreed with the MTT cytotoxicity assay (see Table 1). Cell membrane binding and disintegration induced by these peptides were further observed using confocal microscopy as shown in Fig. 6. The microscopy images demonstrate that Alexa Fluor 488–labeled ribe 31 (Fig. 6*B*) mainly binds to the outer membranes of Sf9 cells in a similar way to fluorescently labeled cyO2 (Fig. 6*A*) at 0.5 μM. Compared to cyO2 and ribe 31, Alexa Fluor 488–labeled kalata B1 binds to the cell membrane to a lesser extent at the same concentration but is internalized into cells more efficiently with no sign of membrane disruption (Fig. 6*C*). Ribe 31 was able to puncture cell membranes and become internalized. Cell membrane disintegration was observed for insect cells incubated with Alexa Fluor 488–labeled ribe 31 and cyO2 at 0.5 μM as indicated by *white* arrows.

Membrane binding properties of ribe peptides

The main phospholipids of larval and prepupal stages of *D. melanogaster* are PE and phosphatidylcholine (45). The dominant membrane phospholipid at both stages of development is PE, constituting 50% to 60% of the total phospholipids. To provide insights into the insecticidal mode of action of ribe peptides against *D. melanogaster*, two model membranes, (i) 1-palmitoyl-2-oleoyl-glycero-3-phosphocholine (POPC) and (ii) a mixture of POPC and 1-palmitoyl-2-oleoyl-sn-glycero-3-phosphoethanolamine (POPE) phospholipids (80:20), were used to study their membrane-binding properties using SPR. All the isolated ribe peptides exhibited strong binding to the

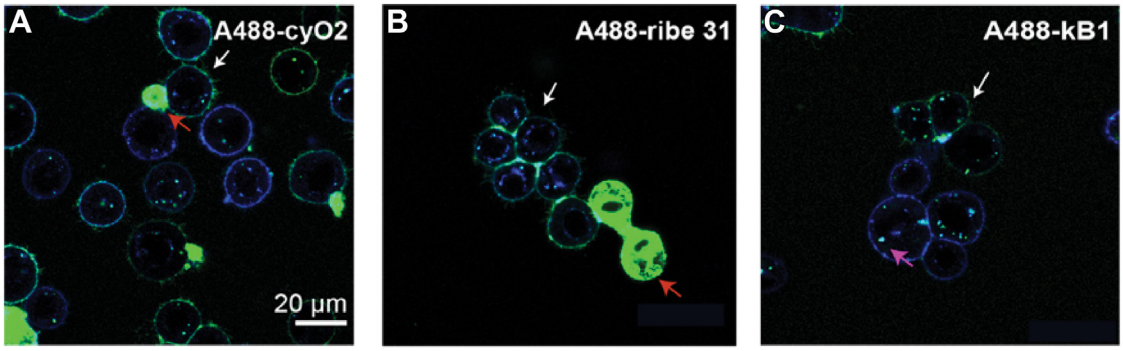

Figure 6. The interactions of Alexa Fluor 488–labeled cystine knot peptides (*green*) with live Sf9 cells were imaged using confocal microscopy. Sf9 insect cells were treated with (*A*) Alexa Fluor 488–labeled cyO2 (A488-cyO2) at 0.5 μM, (*B*) Alexa Fluor 488–labeled ribe 31 (A488-ribe 31) at 0.5 μM, and (*C*) Alexa Fluor 488–labeled kalata B1 (A488-kB1) at 0.5 μM. Images were captured after 30 min of treatment. The cell membrane was labeled with wheat germ agglutinin conjugated with Alexa Fluor 647 (*blue*).

lipid bilayer containing POPC/POPE, which agrees with previous studies reporting the preferential binding of cyclotides toward PE phospholipids (see Table 2 and Fig. 5*B*) (46–48). As expected, the ribe peptides did not bind to the POPC model membrane (Fig. S4), highlighting the requirement of PE phospholipids for binding. Based on peptide-to-lipid maximum binding (P/L max, mol/mol), ribe 31 displayed better binding to POPC/POPE lipids (Table 2, Fig. 5*B*). In contrast, ribe 20 displayed the lowest P/L value (0.30 mol/mol), in agreement with its lower *in vitro* cytotoxicity (Table 1). In summary, the membrane binding molar ratios of the ribe peptides correlate with their cytotoxicity. The membrane-binding potential of ribe 31 provides a mechanistic explanation for its potent *in vivo* activity against *D. melanogaster*.

Discussion

The insecticidal activities and modes of action of cyclotides have been discussed extensively (15, 49–51). Previous studies have shown that the hydrophobicity of cyclotides contributes to their key biological activities, with their surface-exposed hydrophobic patch inserting into, and disrupting, cell membranes (46). For example, the insecticidal activity of cyclotide parigidin-br1 is broadly dependent on its membrane-binding ability for its biological effects. The hydrophobic surface patch interacts with the cell membrane and causes extensive swelling of cells, leading to cell death (13). The membrane lytic activity of cyclotides is linked to both insecticidal and hemolytic activities as reported in an alanine-scanning mutagenesis study of kalata B1 (52). To determine whether the biological activities of acyclotides from *R. bengalensis* depend on their hydrophobicity, the activities of ribe peptides exhibiting a range of values for overall hydrophobicity were evaluated in a series of *in vitro* and *in vivo* assays.

Table 2
Membrane binding of ribe peptides toward two lipid systems determined by surface plasmon resonance

	POPC/POPE (80:20)	
Peptide	P/L max (mol/mol)[a]	K_D (μM)[b]
ribe 10	0.33 ± 0.01	8.9 ± 0.33
ribe 20	0.30 ± 0.00	17.3 ± 0.49
ribe 24	0.37 ± 0.00	6.2 ± 0.18
ribe 31	0.38 ± 0.03	6.4 ± 0.59
ribe 33	0.33 ± 0.00	3.2 ± 0.04
cyO2	0.33 ± 0.00	3.0 ± 0.07
kalata B1	0.27 ± 0.00	10.3 ± 0.12

The P/L max and K_D values for POPC could not be defined (data not shown) as the response curves for binding of isolated peptides to this lipid membrane did not reach a plateau in the tested concentration range (4 μM to 32 μM).
[a] maximum peptide-to-lipid molar binding ratio.
[b] Peptide concentration to achieve half-maximum binding at equilibrium. The SD of the mean was determined by fitting a nonlinear equation (Hill slope).

To provide a baseline to interpret the bioassay data, it was important to determine if the structures of acyclotides are rigid and similar to those of cyclotides, which have been extensively studied. The NMR solution structure of ribe 31 reported here suggests that indeed this acyclotide is rigid in solution and has similar secondary structure elements to cyclotides, specifically a ß-sheet and a series of turns built around the cystine knot core (6). The finding that acyclotides such as ribe 31 have potent insecticidal activity, yet lack a cyclic backbone, indicates that the cystine knot motif is a more dominant structural influence on activity than the cyclic backbone. This finding is in agreement with previous structural studies on cyclotides and synthetic linear analogs (4, 53).

The insect cytotoxic activity of the ribe peptides was tested in MTT assays, and the interaction with the plasma membrane of insect cells was observed using live cell imaging. *In vitro* toxicity tests indicated that all ribe peptides were cytotoxic toward Sf9 (*Spodoptera frugiperda*, a pest of global importance) and High Five insect cells, with only moderate variability between the peptides. Ribe 24 and 31 showed the highest toxicity amongst the acyclotides to Sf9 insect cells, which was expected if using overall high hydrophobicity of a particular ribe peptide to be predictive of insect cytotoxicity. Interestingly, the most late-eluting peptide, ribe 33, displayed lower toxicity than the acyclotides ribe 24 and 31. One potential explanation is that the cyclic backbone of ribe 33 has a significant effect on its elution time, and therefore, the difference in elution times between the cyclotide ribe 33 and the acyclotides ribe 24 and 31 is not a true representation of increased hydrophobic patch density.

The hemolytic activity of the ribe acyclotides against human RBCs was of similar magnitude to that reported previously for

a range of cyclotides, that is, $EC_{50} > 10$ μM (46). The lower toxicity of the ribe peptides toward human RBCs compared to the two insect cell lines suggests that these peptides have a degree of selectivity and hence, with further optimization, would have potential as insecticides with low mammalian toxicity. Simonsen *et al.* (52) reported that the hemolytic activity of kalata B1 can be eradicated or significantly diminished by mutation of a single amino acid in the bioactive and hydrophobic surfaces. Interestingly, ribe 10 and 31 share high sequence similarity except for three residues at positions 16, 21, and 23. However, the acyclotide ribe 10 shows higher lysis to RBCs than the cyclotide ribe 31. Overall, the toxicity results highlight that the presence of a cyclic backbone does not necessarily correlate with high cytotoxicity. Rather, the data suggest that hydrophobicity plays a key role in the biological activity of both cyclotides and acyclotides.

The *in vivo* toxicity of the ribe peptides further supports the hypothesis that the hydrophobicity of cyclotides, extended here to acyclotides, influences their biological activities (46). Ribe 31 is the most toxic and the most hydrophobic acyclotide based on the grand average of hydropathy score. The tested cyclotides and acyclotides bound to and destabilized membrane surfaces containing POPE phospholipids but showed weak permeabilization of membranes lacking POPE. This result suggests that the mechanism of membrane destabilization of acyclotides and cyclotides is related to peptide-lipid recognition and subsequent hydrophobic interactions (46–48). Ribe 31 has a large hydrophobic patch capable of establishing strong contacts with insect cell membranes. Thus, it appears likely that the insecticidal activity of ribe 31 is due to its ability to effectively bind to and disrupt the lipid membrane of *Drosophila* cells. Ribe 10 has only one different residue in loop 3 compared to ribe 31 (Gln *versus* Val), yet ribe 10 has no noticeable *in vivo* activity. Therefore, it is likely that Val18 of ribe 31 contributes to the exposed hydrophobic patch in loop 3, which is key for membrane-binding activity.

Henriques *et al.* (54) proposed that low concentrations of Möbius and bracelet cyclotides are internalized by targeting cell membranes through initial interaction of a conserved Glu in loop 1 with PE phospholipids and insertion into the outer leaflet *via* their hydrophobic patch. At high concentrations, it was proposed that cyclotides enter cells through direct membrane translocation or *via* endocytosis. Ribe 31 (0.5 μM) followed the internalization trend of cyclotides, in that at a low concentration it binds to the outer cell membrane (Fig. 5). The cell necrosis induced by ribe 31 is characterized by a general swelling of the cell and rapid loss of plasma membrane integrity.

In summary, this is the first study to explore the *in vivo* insecticidal activity of acyclotides. The acyclotide ribe 31, of all the peptides tested, showed the greatest potency in *D. melanogaster* and was more potent than the previously reported insecticidal cyclotides cyO2 and kalata B1, with reduced mammalian cell toxicity. A mechanism in which acyclotide ribe 31 targets insect cell membranes through interaction with PE headgroups, followed by insertion into the membrane hydrophobic core and disruption of the cell membrane is supported by the SPR and confocal imaging studies reported here. The observed binding of acyclotides to PE is consistent with their incorporation of a conserved glutamic acid residue in loop 1, which has been identified as the first point of interaction of cyclotides with PE containing membranes (41, 54).

In conclusion, ribe 31 is a promising bioinsecticide lead. NMR structural analysis and stability investigations revealed that this acyclotide adopts the same secondary structural features and has the same stability enhancing characteristics that have stimulated the use of cyclotides as molecular design scaffolds. Given their relative ease of synthesis compared to cyclotides in that no cyclization step is required, acyclotides are an underexplored scaffold for agricultural applications where large scale manufacture would be required. Although less abundant in nature than cyclotides, the potential applications of acyclotides are similarly promising.

Experimental procedures

Extraction and isolation of ribe peptides from the stem and leaf of R. bengalensis

Ribe peptides were individually isolated from stem and leaf of *R. bengalensis* for the *in vitro* and *in vivo* assays. Plant tissues were ground in liquid nitrogen before extraction with 50% MeCN and 1% formic acid in water as previously described (12). The extracts were centrifuged before supernatant filtration and lyophilization. Crude extracts were redissolved in 10% (v/v) MeCN and 1% (v/v) formic acid and applied to a solid phase extraction reversed-phase column for preliminary fractionation. Isolation of cyclotides from 40% to 50% MeCN solid phase extraction fractions was carried out using RP-HPLC. For preparative peptide separations, samples were diluted in 20% (v/v) MeCN and 1% (v/v) TFA and filtered through a 0.45 μm RC membrane filter and loaded onto a preparative Phenomenex C_{18} column. Peptides were further purified using semi-preparative or analytical HPLC. Linear 1%, 0.5%, or 0.25% min^{-1} MeCN gradients were delivered to the column at a flow rate of 8 ml min^{-1} for preparative, 3 ml min^{-1} for semi-preparative, and 1 ml min^{-1} for standard bore separations, respectively. A dual wavelength UV detector set to 214 and 280 nm was used to monitor eluent with fractions collected. The mass of ribe peptides was confirmed by an electrospray ionization mass spectrometry. Acyclotides ribe 10, 20, 24, and 31 and cyclotide ribe 33 were purified to >95% purity through repetitive RP-HPLC and their purity was confirmed by LC-MS. CyO2 and kalata B1, isolated from *Viola odorata* and *O. affinis*, respectively, were used as control peptides for the biological assays in this study.

Cell culture

Insect cells High Five and Sf9 were cultured in ESF 921 (Expression Systems) medium at 27 °C, 5% CO_2 in a 75 cm^2 flask until 80% confluent (27).

Cytotoxicity assay

Ribe peptides and positive controls (cyclotides kalata B1 and cycloviolacin O2) were added in triplicate in concentrations

from 0.2 μM to 20 μM. Cells in control wells were incubated with 0.1% Triton X-100. Three 'media only' wells, which did not contain cells, were also included for background measurement. Cells were incubated for 24 h at 27 °C and 5% CO_2. Ten microliters of MTT (5 mg/ml in PBS) was added to each well to a concentration of 0.5 mg/ml. Plates were then incubated for 3 h at 27 °C, 5% CO_2. Supernatants were removed, and the insoluble formazan crystals were resuspended in 100 μl of dimethyl sulfoxide. The plate was shaken at room temperature for 10 min to fully dissolve the formazan crystals, and the absorbance of the solutions was measured at 600 nm.

Hemolytic assay

Toxicity toward human RBCs from three donors was assessed using the method previously described (12). Fresh RBCs were collected according to protocols approved by the Human Research Ethics Unit of The University of Queensland (approval number 2013000582). Peptides were prepared at concentrations from 0.2 to 25 μM. Melittin (0.03–3.3 μM) was used as a positive control. Cyclotides or melittin were added to 0.25% RBC solutions in a 96-well round bottom plate. Control wells were included in each plate, where cells incubated with 0.1% Triton-X were used as a positive control (maximum hemolysis) and cells with water as a vehicle control. The plates were incubated at 37 °C for 1 h and then spun at 1000 rpm for 5 min. The supernatant from each well was transferred into new flat-bottomed plates, and the absorbance was measured at 405 nm. Experiments were done in triplicate.

In vivo *feeding assay*

All CAFE experiments were performed with 4 to 6 day old mated female Canton S *D. melanogaster* at 23 °C. Flies were starved in vials on agarose overnight prior to the capillary feeding experiments (55). Each experiment was done with 15 flies per vial, with 7 vials used for each experimental condition (n = 105 flies total per condition). The ribe peptides, cyO2 and kalata B1, were dissolved in milliQ water and quantified using a UV-visible spectrophotometer based on their absorbance at 280 nm. Peptide stocks were diluted in 10% or 20% sucrose and food dye solution to the desired concentrations and fed to the flies through capillaries. The number of dead flies in each vial was recorded every 1 or 2 h excluding the night period. Mortality was monitored for up to 25 days. The experimenter (SO) was blinded to peptide identities and concentrations, which were unmasked after analysis (by TTD). Data visualization and analysis was performed by using estimation statistics as described previously (56). Briefly, the survival of individual flies was displayed in scatter plots where the average survival of the control population was compared with survival of flies that were fed different peptide concentrations. Differences in survival between the control and test groups were displayed as Δ Survival time with 95% confidence interval.

Structural analysis by NMR

Peptides were prepared for NMR analysis by dissolving in 90% H_2O/10% D_2O (v/v) at a concentration of 1 mM. ^{1}H NMR 2D spectra (TOCSY and NOESY) were recorded at mixing times of 80 and 200 ms, respectively, on a Bruker Avance III 600 MHz spectrometer equipped with a cryoprobe at 298 K. Spectra were referenced internally to 4,4-dimethyl-4-silapentane-1-sulfonic acid. NMR data were processed using TOPSPIN 3.6.1 (Bruker), and assignments were made using CCPNMR (version 2.4.4). Additional spectra were acquired for ribe 31 to determine its three-dimensional structure, including TOCSY spectra at variable temperatures (283–303K) and indirect heteronuclear experiments (^{1}H-^{15}N heteronuclear single quantum coherence [HSQC] and ^{1}H-^{13}C HSQC). Initial structures of ribe 31 were calculated using the program CYANA with NOESY-derived distance restraints, distance restraints to define the C_I-C_{IV}, C_{II}-C_V, C_{III}-C_{VI} connectivity, and backbone Φ and ψ dihedral angles generated using the program TALOS-N (57). Hydrogen bond pairs were added based upon preliminary structures and amide temperature coefficients (58). CNS (59) was used to generate a final set of structures using torsion angle dynamics with refinement and energy minimization in explicit solvent; final structures were assessed for stereochemical quality using MolProbity (60).

Cytotoxicity of peptides visualized using confocal microscopy

Sf9 insect cells were seeded in 8-well borosilicate plates (Thermo Fisher Scientific) at 10,000 cells/well, the day prior to the assay. Right before the experiment, the medium was replaced with phenol red–free Dulbecco's modified Eagle's medium (DMEM) medium containing SYTOX Green. Live cell imaging started immediately after Sf9 cells were treated with acyclotide ribe 31 at 1 μM. Images were captured using a 20 × 0.45 NA S Plan Fluor ELWD objective and SYTOX Green fluorescence signal was amplified using a 525/30 nm band-pass filter. Images were captured every 60 s for 4 h using a custom built inverted widefield Nikon deconvolution microscopy and were analyzed and exported using FIJI software (https://fiji.sc/) (61). Cells were incubated at 27 °C with 5% CO_2 during the imaging process.

Peptide–membrane interaction visualized using confocal imaging

To visualize the interaction of ribe 33 and kalata B1 and cyO2 with insect cells, Sf9 insect cells were seeded in 8-well borosilicate plates (Thermo Fisher Scientific) at 15,000 cells/well, 1 day prior to the assay. Immediately before the experiment, the medium was replaced with phenol red–free DMEM medium containing wheat germ agglutinin Alexa-647 conjugate (1:500, v/v), and cells were treated with Alexa Fluor 488–labeled ribe 31, cyO2, or kalata B1 at 0.5 μM, individually. Images were captured after 1 h treatment on Zeiss 880 LSM confocal equipped with a 63x 1.4 NA Plan Apochromat objective running Zeiss Zen Black software. The microscopy images were analyzed using FIJI software (61). Cells were incubated at 27 °C with 5% CO_2 during the imaging process.

Lipid binding of ribe peptides evaluated using SPR

Synthetic lipids POPC and POPE were purchased from Avanti Polar Lipids. Two model membranes were prepared:

POPC and POPC/POPE (80:20, mol/mol) using the method described previously (61). Briefly, small unilamellar vesicles resuspended in Hepes buffer (10 mM Hepes, 150 mM NaCl, pH 7.4, filtered) were obtained using a mini extruder (Avanti) with a 50 nm polycarbonate membrane. Membrane binding of acyclotides and cyclotides toward POPC or POPC/POPE was evaluated using an L1 sensor chip on a Biacore T200 instrument. A suspension of small unilamellar vesicles (0.5 mM) was deposited onto an L1 chip surface at 2 μl/min for 40 min, followed by a short pulse of 10 mM NaOH. The cyclotide solutions were injected over the lipid surface at 5 μl/min for 180 s, and the dissociation process was recorded for 10 min. Dose–response curves were established through the calculated peptide-to-lipid molar ratio to evaluate the binding ability of the tested peptides. K_D was calculated by fitting in specific binding with Hill slope using GraphPad Prism software (GraphPad Software Inc) (61).

Data availability

Three-dimensional structural data and chemical shifts of ribe 31 have been deposited (PDB ID 7KPD, BMRB Accession No. 30813).

Supporting information—The supporting information is available free of charge (62).

Acknowledgments—This work was supported by grants from the Australian Research Council (DP150100443 and DP200101299) and by access to the facilities of the Australian Research Council (ARC) Centre of Excellence for Innovations in Peptide and Protein Science (CE200100012). The work was facilitated using infrastructure provided by the Australian Government through the National Collaborative Research Infrastructure strategy (NCRIS). Microscopy was performed at the Australian Cancer Research Foundation (ACRF)/ Institute for Molecular Bioscience Cancer Biology Imaging Facility.

Author contributions—A. C. C. and D. J. C. conceptualization; T. T. D., Y. H. H., S. O., P. J. H., E. K. G., and L. Y. C. methodology; Q. K. software; Q. K. validation; T. T. D., Y. H. H., S. O., P. J. H., and E. K. G. formal analysis; T. T. D., Y. H. H., S. O., P. J. H., E. K. G., L. Y. C., A. C. C., and D. J. C. investigation; A. C. C. and D. J. C. resources; T. T. D., Y. H. H., S. O., P. J. H., E. K. G., L. Y. C., B. J. T., and Q. K. writing–original draft; T. T. D., Y. H. H., S. O., P. J. H., E. K. G., L. Y. C., Q. K., A. C. C., and D. J. C. writing–review & editing; T. T. D. and S. O. visualization; Y. H. H., L. Y. C., Q. K., A. C. C., and D. J. C. supervision; L. Y. C. project administration; A. C. C. and D. J. C. funding acquisition.

Funding and additional information—L. Y. C was supported by the Advance Queensland Women's Academic Fund (WAF-6884942288) and D. J. C is an NHMRC Leadership Fellow (GNT2009564). A. C. C. and S. O. were supported by grants from the Singapore Ministry of Education (MOE2017-T2-1-089) and by Duke-NUS Medical School.

Conflict of interest—The authors declare that they have no conflicts of interest with the contents of this article.

Abbreviations—The abbreviations used are: MTT, 3-(4,5-dimethylthiazol-2-yl)-2,5-diphenyl-tetrazolium bromide; PE, phosphatidyl-ethanolamine; POPC, 1-palmitoyl-2-oleoyl-glycero-3-phosphocholine; POPE, 1-palmitoyl-2-oleoyl-sn-glycero-3-phosphoethanolamine; RBC, red blood cell; RP-HPLC, reverse-phase HPLC; SPR, surface plasmon resonance.

References

1. Craik, D. J., Daly, N. L., Bond, T., and Waine, C. (1999) Plant cyclotides: a unique family of cyclic and knotted proteins that defines the cyclic cystine knot structural motif. *J. Mol. Biol.* **294**, 1327–1336
2. de Veer, S. J., Kan, M. W., and Craik, D. J. (2019) Cyclotides: from structure to function. *Chem. Rev.* **119**, 12375–12421
3. Wang, C. K., and Craik, D. J. (2018) Designing macrocyclic disulfide-rich peptides for biotechnological applications. *Nat. Chem. Biol.* **14**, 417–427
4. Colgrave, M. L., and Craik, D. J. (2004) Thermal, chemical, and enzymatic stability of the cyclotide kalata B1: the importance of the cyclic cystine knot. *Biochemistry* **43**, 5965–5975
5. Hernandez, J. F., Gagnon, J., Chiche, L., Nguyen, T. M., Andrieu, J. P., Heitz, A., *et al.* (2000) Squash trypsin inhibitors from *Momordica cochinchinensis* exhibit an atypical macrocyclic structure. *Biochemistry* **39**, 5722–5730
6. Craik, D. J. (2012) Host-defense activities of cyclotides. *Toxins* **4**, 139–156
7. Simonsen, S. M., Sando, L., Ireland, D. C., Colgrave, M. L., Bharathi, R., Göransson, U., *et al.* (2005) A continent of plant defense peptide diversity: cyclotides in Australian *Hybanthus* (Violaceae). *Plant Cell* **17**, 3176–3189
8. Nguyen, K. N. T., Nguyen, G. K. T., Nguyen, P. Q. T., Ang, K. H., Dedon, P. C., and Tam, J. P. (2016) Immunostimulating and Gram-negative-specific antibacterial cyclotides from the butterfly pea (*Clitoria ternatea*). *FEBS J.* **283**, 2067–2090
9. Porto, W. F., Pires, A. S., and Franco, O. L. (2012) CS-AMPPred: an updated SVM model for antimicrobial activity prediction in cysteine-stabilized peptides. *PLoS One* **7**, e51444
10. Pränting, M., Lööv, C., Burman, R., Göransson, U., and Andersson, D. I. (2010) The cyclotide cycloviolacin O2 from *Viola odorata* has potent bactericidal activity against Gram-negative bacteria. *J. Antimicrob. Chemother.* **65**, 1964–1971
11. Göransson, U., Sjögren, M., Svangård, E., Claeson, P., and Bohlin, L. (2004) Reversible antifouling effect of the cyclotide cycloviolacin O2 against barnacles. *J. Nat. Prod.* **67**, 1287–1290
12. Dang, T. T., Chan, L. Y., Huang, Y. H., Nguyen, L. T. T., Kaas, Q., Huynh, T., *et al.* (2020) Exploring the sequence diversity of cyclotides from Vietnamese viola species. *J. Nat. Prod.* **83**, 1817–1828
13. Pinto, M. F. S., Fensterseifer, I. C. M., Migliolo, L., Sousa, D. A., de Capdville, G., Arboleda-Valencia, J. W., *et al.* (2012) Identification and structural characterization of novel cyclotide with activity against an insect pest of sugar cane. *J. Biol. Chem.* **287**, 134–147
14. Plan, M. R. R., Saska, I., Cagauan, A. G., and Craik, D. J. (2008) Backbone cyclised peptides from plants show molluscicidal activity against the rice pest *Pomacea canaliculata* (golden apple snail). *J. Agric. Food Chem.* **56**, 5237–5241
15. Jennings, C., West, J., Waine, C., Craik, D., and Anderson, M. (2001) Biosynthesis and insecticidal properties of plant cyclotides: the cyclic knotted proteins from *Oldenlandia affinis*. *Proc. Natl. Acad. Sci. U. S. A.* **98**, 10614–10619
16. Dancewicz, K., Slazak, B., Kielkiewicz, M., Kapusta, M., Bohdanowicz, J., and Gabrys, B. (2020) Behavioral and physiological effects of Viola spp. cyclotides on Myzus persicae (Sulz.). *J. Insect Physiol.* **122**, 104025
17. Poth, A. G., Colgrave, M. L., Lyons, R. E., Daly, N. L., and Craik, D. J. (2011) Discovery of an unusual biosynthetic origin for circular proteins in legumes. *Proc. Natl. Acad. Sci. U. S. A.* **108**, 10127–10132
18. Tammineni, R., Gulati, P., Kumar, S., and Mohanty, A. (2020) An overview of acyclotides: past, present and future. *Phytochemistry* **170**, 112215
19. Nguyen, G. K., Lian, Y. L., Pang, E. W. H., Phuong, Q. T. N., Tran, T. D., and Tam, J. P. (2013) Discovery of linear cyclotides in monocot plant *Panicum laxum* of Poaceae family provides new insights into evolution and distribution of cyclotides in plants. *J. Biol. Chem.* **288**, 3370–3380
20. Dang, T. T., Chan, L. Y., Tombling, B. J., Harvey, P. J., Gilding, E. K., and Craik, D. J. (2021) Planta discovery and chemical synthesis of bracelet cystine knot peptides from Rinorea bengalensis. *J. Nat. Prod.* **84**, 395–407

21. Jackson, M. A., Gilding, E. K., Shafee, T., Harris, K. S., Kaas, Q., Poon, S., *et al.* (2018) Molecular basis for the production of cyclic peptides by plant asparaginyl endopeptidases. *Nat. Commun.* **9**, 2411
22. Ireland, D. C., Colgrave, M. L., Nguyencong, P., Daly, N. L., and Craik, D. J. (2006) Discovery and characterization of a linear cyclotide from *Viola odorata*: implications for the processing of circular proteins. *J. Mol. Biol.* **357**, 1522–1535
23. Mylne, J. S., Chan, L. Y., Chanson, A. H., Daly, N. L., Schaefer, H., Bailey, T. L., *et al.* (2012) Cyclic peptides arising by evolutionary parallelism via asparaginyl-endopeptidase–mediated biosynthesis. *Plant Cell* **24**, 2765–2778
24. Wang, C. K., Kaas, Q., Chiche, L., and Craik, D. J. (2008) CyBase: a database of cyclic protein sequences and structures, with applications in protein discovery and engineering. *Nucleic Acids Res.* **36**, D206–D210
25. Mulvenna, J. P., Wang, C., and Craik, D. J. (2006) CyBase: a database of cyclic protein sequence and structure. *Nucleic Acids Res.* **34**, D192–D194
26. Plan, M. R. R., Göransson, U., Clark, R. J., Daly, N. L., Colgrave, M. L., and Craik, D. J. (2007) The cyclotide fingerprint in *Oldenlandia affinis*: elucidation of chemically modified, linear and novel macrocyclic peptides. *ChemBioChem* **8**, 1001–1011
27. Du, J., Chan, L. Y., Poth, A. G., and Craik, D. J. (2019) Discovery and characterization of cyclic and acyclic trypsin inhibitors from *Momordica dioica*. *J. Nat. Prod.* **82**, 293–300
28. Hossard, L., Philibert, A., Bertrand, M., Colnenne-David, C., Debaeke, P., Munier-Jolain, N., *et al.* (2014) Effects of halving pesticide use on wheat production. *Sci. Rep.* **4**, 4405
29. Braga, A. R. C., de Rosso, V. V., Harayashiki, C. A. Y., Jimenez, P. C., and Castro, Í. B. (2020) Global health risks from pesticide use in Brazil. *Nat. Food* **1**, 312–314
30. Gill, J. P. S., Bedi, J. S., Singh, R., Fairoze, M. N., Hazarika, R. A., Gaurav, A., *et al.* (2020) Pesticide residues in peri-urban bovine milk from India and risk assessment: a multicenter study. *Sci. Rep.* **10**, 8054
31. Wang, N., Jiang, Q., Han, L., Zhang, H., Zhu, B., and Liu, X. (2019) Epidemiological characteristics of pesticide poisoning in Jiangsu Province, China, from 2007 to 2016. *Sci. Rep.* **9**, 8604
32. Goodhue, R. E., Bolda, M., Farnsworth, D., Williams, J. C., and Zalom, F. G. (2011) Spotted wing drosophila infestation of California strawberries and raspberries: Economic analysis of potential revenue losses and control costs. *Pest Manag. Sci.* **67**, 1396–1402
33. Riaz, B., Zahoor, M. K., Zahoor, M. A., Majeed, H. N., Javed, I., Ahmad, A., *et al.* (2018) Toxicity, phytochemical composition, and enzyme inhibitory activities of some indigenous weed plant extracts in fruit fly, Drosophila melanogaster. *Evid. Based Complement. Alternat. Med.* **2018**, 2325659
34. Tolwinski, N. S. (2017) Introduction: Drosophila-A model system for developmental Biology. *J. Dev. Biol.* **5**, 9
35. Scott, J. G., and Buchon, N. (2019) Drosophila melanogaster as a powerful tool for studying insect toxicology. *Pestic. Biochem. Physiol.* **161**, 95–103
36. Akmoutsou, P., Mademtzoglou, D., Nakou, I., Onoufriadis, A., Papadopoulou, X., Kounatidis, I., *et al.* (2011) Evaluation of toxicity and genotoxic effects of spinosad and deltamethrin in Drosophila melanogaster and Bactrocera oleae. *Pest Manag. Sci.* **67**, 1534–1540
37. Muñoz, E., Lamilla, C., Marin, J. C., Alarcon, J., and Cespedes, C. L. (2013) Antifeedant, insect growth regulatory and insecticidal effects of Calceolaria talcana (Calceolariaceae) on Drosophila melanogaster and Spodoptera frugiperda. *Ind. Crops Prod.* **42**, 137–144
38. Chowanski, S., Chudzinska, E., Lelario, F., Ventrella, E., Marciniak, P., Miadowicz-Kobielska, M., *et al.* (2018) Insecticidal properties of Solanum nigrum and Armoracia rusticana extracts on reproduction and development of Drosophila melanogaster. *Ecotoxicol. Environ. Saf.* **162**, 454–463
39. Ffrench-Constant, R. H. (2013) The molecular genetics of insecticide resistance. *Genetics* **194**, 807–815
40. Strycharz, J. P., Lao, A., Li, H., Qiu, X., Lee, S. H., Sun, W., *et al.* (2013) Resistance in the highly DDT-resistant 91-R strain of Drosophila melanogaster involves decreased penetration, increased metabolism, and direct excretion. *Pestic. Biochem. Physiol.* **107**, 207–217
41. Göransson, U., Herrmann, A., Burman, R., Haugaard-Jönsson, L. M., and Rosengren, K. J. (2009) The conserved Glu in the cyclotide cycloviolacin O2 has a key structural role. *ChemBioChem* **10**, 2354–2360
42. Jaspard, E., Macherel, D., and Hunault, G. (2012) Computational and statistical analyses of amino acid usage and physico-chemical properties of the twelve late embryogenesis abundant protein classes. *PLoS One* **7**, e36968
43. Colgrave, M. L., Kotze, A. C., Huang, Y. H., O'Grady, J., Simonsen, S. M., and Craik, D. J. (2008) Cyclotides: natural, circular plant peptides that possess significant activity against gastrointestinal nematode parasites of sheep. *Biochemistry* **47**, 5581–5589
44. Colgrave, M. L., Kotze, A. C., Ireland, D. C., Wang, C. K., and Craik, D. J. (2008) The anthelmintic activity of the cyclotides: natural variants with enhanced activity. *ChemBioChem* **9**, 1939–1945
45. Jones, H. E., Harwood, J. L., Bowen, I. D., and Griffiths, G. (1992) Lipid composition of subcellular membranes from larvae and prepupae of Drosophila melanogaster. *Lipids* **27**, 984–987
46. Henriques, S. T., and Craik, D. J. (2012) Importance of the cell membrane on the mechanism of action of cyclotides. *ACS Chem. Biol.* **7**, 626–636
47. Henriques, S. T., Huang, Y. H., Castanho, M. A. R. B., Bagatolli, L. A., Sonza, S., Tachedjian, G., *et al.* (2012) Phosphatidylethanolamine binding is a conserved feature of cyclotide-membrane interactions. *J. Biol. Chem.* **287**, 33629–33643
48. Henriques, S. T., Huang, Y.-H., Chaousis, S., Wang, C. K., and Craik, D. J. (2014) Anticancer and toxic properties of cyclotides are dependent on phosphatidylethanolamine phospholipid targeting. *ChemBioChem* **15**, 1956–1965
49. Broussalis, A. M., Clemente, S., and Ferraro, G. E. (2010) *Hybanthus parviflorus* (Violaceae): Insecticidal activity of a south American plant. *Crop Prot.* **29**, 953–956
50. Gruber, C. W., Čemažar, M., Anderson, M. A., and Craik, D. J. (2007) Insecticidal plant cyclotides and related cystine knot toxins. *Toxicon* **49**, 561–575
51. Jennings, C. V., Rosengren, K. J., Daly, N. L., Plan, M., Stevens, J., Scanlon, M. J., *et al.* (2005) Isolation, solution structure, and insecticidal activity of kalata B2, a circular protein with a twist: do möbius strips exist in nature? *Biochemistry* **44**, 851–860
52. Simonsen, S. M., Sando, L., Rosengren, K. J., Wang, C. K., Colgrave, M. L., Daly, N. L., *et al.* (2008) Alanine scanning mutagenesis of the prototypic cyclotide reveals a cluster of residues essential for bioactivity. *J. Biol. Chem.* **283**, 9805–9813
53. Wang, C. K., Hu, S. H., Martin, J. L., Sjogren, T., Hajdu, J., Bohlin, L., *et al.* (2009) Combined X-ray and NMR analysis of the stability of the cyclotide cystine knot fold that underpins its insecticidal activity and potential use as a drug scaffold. *J. Biol. Chem.* **284**, 10672–10683
54. Henriques, S. T., and Craik, D. J. (2017) Cyclotide structure and function: the role of membrane binding and permeation. *Biochemistry* **56**, 669–682
55. Diegelmann, S., Jansen, A., Jois, S., Kastenholz, K., Velo Escarcena, L., Strudthoff, N., *et al.* (2017) The CApillary FEeder assay measures food intake in Drosophila melanogaster. *J. Vis. Exp.* **121**, 55024
56. Ho, J., Tumkaya, T., Aryal, S., Choi, H., and Claridge-Chang, A. (2019) Moving beyond P values: Data analysis with estimation graphics. *Nat. Methods* **16**, 565–566
57. Shen, Y., and Bax, A. (2013) Protein backbone and sidechain torsion angles predicted from NMR chemical shifts using artificial neural networks. *J. Biomol. NMR* **56**, 227–241
58. Cierpicki, T., and Otlewski, J. (2001) Amide proton temperature coefficients as hydrogen bond indicators in proteins. *J. Biomol. NMR* **21**, 249–261
59. Brunger, A. T. (2007) Version 1.2 of the crystallography and NMR system. *Nat. Protoc.* **2**, 2728–2733
60. Chen, V. B., Arendall, W. B., 3rd, Headd, J. J., Keedy, D. A., Immormino, R. M., Kapral, G. J., *et al.* (2010) MolProbity: All-atom structure validation for macromolecular crystallography. *Acta Crystallogr. D Biol. Crystallogr.* **66**, 12–21
61. Du, Q., Chan, L. Y., Gilding, E. K., Henriques, S. T., Condon, N. D., Ravipati, A. S., *et al.* (2020) Discovery and mechanistic studies of cytotoxic cyclotides from the medicinal herb Hybanthus enneaspermus. *J. Biol. Chem.* **295**, 10911–10925
62. Wang, C. K., Colgrave, M. L., Ireland, D. C., Kaas, Q., and Craik, D. J. (2009) Despite a conserved cystine knot motif, different cyclotides have different membrane binding modes. *Biophys. J.* **97**, 1471–1481